

Axial-vector contributions to the HFS of muonic hydrogen

A. Miranda and P. Roig

Departamento de Física, Centro de Investigación y de Estudios Avanzados del IPN,
Apartado Postal 14-740, 07000 Ciudad de México, México

P. Sánchez-Puertas

Institut de Física d'Altes Energies (IFAE), The Barcelona Institute of Science and Technology (BIST),
Campus UAB, E-08193 Bellaterra (Barcelona), Spain

Received 29 December 2021; accepted 21 April 2022

We review the axial-vector meson contributions to the HFS of muonic hydrogen. We evaluate the impact of the singly- and doubly-virtual asymptotic behavior of the transition form factors of the axial-vector mesons. As our main result, we find an opposite sign (and a factor of 2 difference) concerning previous analyses and a novel discussion of the hadronic modeling.

Keywords: Hyperfine splitting; form factor; axial-vector meson; muonic hydrogen.

DOI: <https://doi.org/10.31349/SuplRevMexFis.3.020719>

1. Introduction

An exhaustive analysis of bound states involving muon leptons, such as muonic hydrogen, is mandatory in view of the existing discrepancies in muon physics [1–5] pointing towards lepton flavor universality violation (LFUV). The measurements performed by the CREMA collaboration allow to extract the value of hyperfine splitting of the $2S$ level [6], $\Delta E_{exp}^{HFS} = 22.8089(51)$ meV, and also several experimental groups are planning to measure the hyperfine structure (HFS) of various muonic atoms with even higher precision [7–9].

The electromagnetic contributions from axial-vector mesons have become relevant recently. Especially, in the context of the hadronic light-by-light (HLbL) contribution to the muon anomalous magnetic moment (a_μ) [10–20], but also regarding their contribution to the HFS of muonic hydrogen [21, 23].

The paper is organized as follows. In Sec. 2, we discuss the amplitude for $A \rightarrow \ell^+ \ell^-$ decays. The axial contributions to the HFS are shown in Sec. 3. In Sec. 4, we describe our particular model based on resonance saturation. Finally, our conclusions are presented in Sec. 5.

2. $A \rightarrow \ell^+ \ell^-$ decays

The leptonic axial-vector meson decays appear as an intermediate step in our calculation, and deserve their own attention as they can provide information about the $A \rightarrow \gamma^* \gamma^*$ transitions [18, 24].

The most general structure for the $A \rightarrow \gamma^* \gamma^*$ transition, which complies with gauge and Lorentz invariance, is given by [12]

$$\begin{aligned} i\mathcal{M}_{A \rightarrow \gamma^* \gamma^*} &= ie^2 \left\{ B_2(q_1^2, q_2^2) i\epsilon_{\mu\alpha\rho\beta} q_1^\beta [q_2^\alpha q_{2\nu} - g_\nu^\alpha q_2^2] \right. \\ &\quad + B_2(q_2^2, q_1^2) i\epsilon_{\nu\alpha\rho\beta} q_2^\beta [q_1^\alpha q_{1\mu} - g_\mu^\alpha q_1^2] \\ &\quad \left. + i\epsilon_{\mu\nu\alpha\beta} q_1^\alpha q_2^\beta [\bar{q}_{12\rho} C_A(q_1^2, q_2^2) + q_{12\rho} C_S(q_1^2, q_2^2)] \right\} (1) \\ &\quad \times \epsilon^{*\mu}(q_1) \epsilon^{*\nu}(q_2) \epsilon^\rho(q_{12}) \\ &\equiv ie^2 \mathcal{M}_{A\mu\nu\rho} \epsilon^{*\mu}(q_1) \epsilon^{*\nu}(q_2) \epsilon^\rho(q_{12}), \end{aligned}$$

where $q_{12} = q_1 + q_2 = q$, $\bar{q}_{12} = q_1 - q_2$ and $\epsilon^{0123} = +1$. Here, $\epsilon^{*\mu}(q_1)$ and $\epsilon^{*\nu}(q_2)$ are the polarization vectors of the photons, while $\epsilon^\rho(q)$ is the polarization vector of the axial-vector meson with $A = a_1, f_1^{(1)}$. $B_2(q_1^2, q_2^2)$, $C_A(q_1^2, q_2^2)$ and $C_S(q_1^2, q_2^2)$ are form factors. To guarantee the Bose symmetry, $C_A(q_1^2, q_2^2)$ must be antisymmetric and $C_S(q_1^2, q_2^2)$ must be symmetric under $q_1 \leftrightarrow q_2$. The contribution from C_S vanishes when the axial meson is on-shell and, in this basis, can be omitted when considering high-energy constraints [15]ⁱ. In the last expression, C_A corresponds to transversal photons (TT) and B_2 is a combination of TT and LT polarization statesⁱⁱ. In the following, we will use form factors with well-defined symmetry [12, 15]: $B_2(q_1^2, q_2^2) = B_{2S}(q_1^2, q_2^2) + B_{2A}(q_1^2, q_2^2)$ and $B_2(q_2^2, q_1^2) = B_{2S}(q_1^2, q_2^2) - B_{2A}(q_1^2, q_2^2)$.

In Fig. 1, we can see the leading order contribution to the $A \rightarrow \ell^+ \ell^-$ decays. Using Eq. (1), the corresponding amplitude reads as

$$\begin{aligned} i\mathcal{M} &= -e^4 \varepsilon_\rho \int \frac{d^4 k}{(2\pi)^4} \frac{\bar{u}\gamma_\nu[(\not{k} - \not{p}) + m_\ell]\gamma_\mu v}{q_1^2 q_2^2 [(k - p)^2 - m_\ell^2]} \mathcal{M}_A^{\mu\nu\rho}(q_1, q_2) \\ &= i \bar{u}(q - p) [A_1(q^2) \gamma^\rho + A_2(q^2) q^\rho] \gamma^5 v(p) \epsilon_\rho(q), \end{aligned} \quad (2)$$

with $q_1 = k$ and $q_2 = q - k$. The second line in Eq. (2) corresponds to the most general amplitude for these decays,

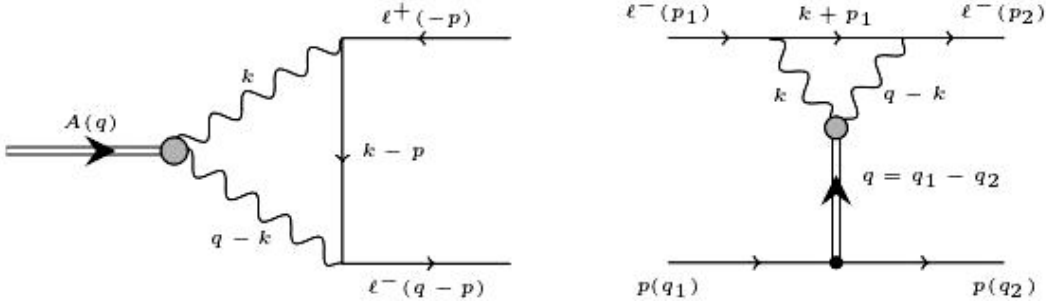


FIGURE 1. The leading contribution to $A \rightarrow \ell^+ \ell^-$ decays (left). The axial-vector meson contribution to the $\ell^- p \rightarrow \ell^- p$ amplitude relevant to the HFS (right). The grey blob includes structure-dependent axial-photon-photon interactions.

TABLE I. Branching fraction for $f_1 \rightarrow e^+ e^-$ decays in units of 10^{-9} with the different form factors outlined in Appendix A (ideal mixing case). In particular the first three columns correspond to models incorporating a vector meson mass $m_V = 0.77$ GeV, whereas the last three columns have effective masses around 1 GeV, illustrating the relevance of the intermediate $V\gamma$ state.

	VMD	eVMD	heVMD	DIP	heDIP	OPE
$\mathcal{B}_{e^+ e^-}$	1.90(⁹²) ₇₄	1.55(⁵⁰) ₃₈	1.66(⁴⁵) ₄₂	2.87(^{3.69}) _{1.73}	2.73(^{3.86}) _{1.69}	2.67(^{3.99}) _{1.75}

where both A_1 and A_2 can be obtained through the projectors in App. A in Ref. [25]. The A_2 amplitude does not contribute to the decay width since it is a pure off-shell effect.

The branching ratios for the $f_1 \rightarrow e^+ e^-$ decays are summarized in Table I using different parameterizations of B_{2S} in Appendix A. These results are compatible with the measurement reported by the SND collaboration [26], $\mathcal{B}(f_1(1285) \rightarrow e^+ e^-) = (5.1^{+3.7})_{-2.7} \cdot 10^{-9}$. Contrary to the $\pi(\eta) \rightarrow \ell^+ \ell^-$ decays, where the imaginary part is dominated by the intermediate 2γ state, the $A \rightarrow \ell^+ \ell^-$ decays are especially sensitive to the intermediate $V\gamma$ contribution as consequence of the Landau-Yang theorem [27, 28].

3. Axial contributions to the HFS

The relevant amplitude for the $\ell^- p \rightarrow \ell^- p$ scattering mediated by axial-vector mesons, Fig. 1(right-hand), can be written as

$$i\mathcal{M}_{\ell p} = ig_{ANN}[\bar{u}\gamma^\nu\gamma^5 u]_N \frac{-g_{\mu\nu} + \frac{q_\mu q_\nu}{m_A^2}}{q^2 - m_A^2} \times [\bar{u}(A_1\gamma^\mu + A_2q^\mu)\gamma^5 u]_e, \quad (3)$$

where the coupling of the axial-vector mesons to the nucleons, g_{ANN} , is introduced through

$$\begin{aligned} \mathcal{L}_{a_1 NN} &= -g_{a_1 NN}(\bar{N}\gamma_\mu\gamma^5\vec{\sigma}N)\vec{a}_1^\mu, \\ \mathcal{L}_{f_1 NN} &= -g_{f_1 NN}(\bar{N}\gamma_\mu\gamma^5 N)f_1^\mu. \end{aligned} \quad (4)$$

Making use of the relation $\mathcal{M}_{\ell p} = -2m_\ell 2m_N \tilde{V}_{NR}(\mathbf{q}^2)$, we obtain the leading expression for the nonrelativistic potential

$$\begin{aligned} \tilde{V}_{NR}(\mathbf{q}^2) &\simeq g_{ANN} \frac{A_1(0)}{m_A^2 + \mathbf{q}^2} (\hat{\sigma}_\ell \cdot \hat{\sigma}_N), \\ V_{NR}(r) &= \frac{g_{ANN} A_1(0)}{4\pi r} e^{-m_A r} (\hat{\sigma}_\ell \cdot \hat{\sigma}_N). \end{aligned} \quad (5)$$

For the HFS, we are interested in the energy difference amongst the $nS_{1/2}^{F=1}$ and the $nS_{1/2}^{F=0}$ energy levels [29]. In particular, for $n = 1, 2$, we get

$$\Delta E_1^{\text{HFS}} = \frac{g_{ANN} A_1(0)}{\pi} \frac{(\mu\alpha)^3}{m_A^2} \frac{4}{(1 + \frac{2\mu\alpha}{m_A})^2}, \quad (6)$$

$$\Delta E_2^{\text{HFS}} = \frac{g_{ANN} A_1(0)}{4\pi} \frac{(\mu\alpha)^3}{m_A^2} \frac{2 + (\frac{\mu\alpha}{m_A})^2}{(1 + \frac{\mu\alpha}{m_A})^4}, \quad (7)$$

to leading order in α^{iii} , where μ is the reduced mass. We note that $A_1(0)$ can be expressed following the notation in Ref. [21] as

$$A_1(0) = \frac{4}{3} \left(\frac{\alpha}{\pi}\right)^2 \int_0^\infty dk^2 L_\ell(k^2) B_{2S}(-k^2, -k^2), \quad (8)$$

with $L_\ell(k^2)$ defined in Ref. [21] (see Eq. (14) therein).^{iv} Likewise, it is straightforward to check that the general results in Ref. [21] amount to our Eqs. (6) and (7) times a factor of (-2) . While we could not trace the factor of 2, the relative sign appears comparing to their Eqs. (5), (20). Still, the sign depends on their photon momentum flow and ϵ^{0123} convention, that are unclear. More importantly, the final sign arising from Eqs. (6) to (8) will depend on the relative sign for $B_{2S}(0, 0)$ and g_{ANN} , that was fixed in Ref. [21] on the basis of quark-loop models.

4. Model results

To determine the contribution to the HFS in Eqs. (6), (7) the sign of $g_{ANN} A_1(0)$ is required which, for our form factors, relates to the the sign of $B_{2S} g_{ANN}$. In this respect, the short-distance constraints obtained from the operator product expansion (OPE) of two vector currents allow to fix $\text{sgn } B_{2S}(0,0) = \text{sgn } F_A m_A$, and thus reducing the problem to determine the sign for $F_A^a m_A g_{ANN}$. This combination appears in the axial form factor of the proton,

$$\begin{aligned} \langle p(k') | \bar{q} \gamma_\mu \gamma^5 \lambda^a q | p(k) \rangle &= \bar{u}(k') \left[\gamma_\mu G_A^a(q^2) \right. \\ &\quad \left. + \frac{q_\mu}{2m_N} G_P^a(q^2) \right] \gamma^5 u(k), \quad (a = 3, 8, 0), \end{aligned} \quad (9)$$

after adopting a resonance saturation scheme. In particular, one finds [22]

$$G_A^a(q^2) = \sum_A \frac{2F_A^a m_A g_{ANN}}{m_A^2 - q^2}, \quad (10)$$

where the sum goes over the (infinite number of) axial-vector meson resonances. Truncating the last expression with the lightest resonance, the value of g_{ANN} can be determined in terms of $G_A^a(0)$. This implies,

$$\begin{aligned} g_{a_1 NN} &= 5.6(1.1), & g_{f_1 NN} &= 2.01(0.17), \\ g_{f'_1 NN} &= -0.33(0.08), & (\phi = 0), \end{aligned} \quad (11)$$

$$\begin{aligned} g_{a_1 NN} &= 5.6(1.1), & g_{f_1 NN} &= 1.93(0.16), \\ g_{f'_1 NN} &= 0.71(21), & (\phi_{L3} = 26.7(5.0)^\circ), \end{aligned} \quad (12)$$

where we have used $g_A^3 = 1.2730(13)$ [30], $g_A^8 = 0.530(18)$, $g_A^0 = 0.392(24)$ [31], $F_A = 140(10)$ MeV [15, 32, 33], $\phi_{L3} = 26.7(5.0)^\circ$ [34, 35] and the PDG [36] masses with an additional uncertainty accounting for the half-width rule [37]. Here, ϕ is the $f_1 - f'_1$ mixing angle in the flavor basis.

The axial-vector contribution to the HFS of muonic hydrogen is shown in Table II where the values from the OPE column in Table III and the coupling in Eq. (11) have been used. Additionally, we have also included the uncertainty related to the mixing angle, ϕ , within brackets.

5. Results and conclusions

In addition to the results for the HFS in Table II, we have incorporated a systematic uncertainty related to the inclusion of a second multiplet of heavier resonances in Eq. (10). Thus,

$$\begin{aligned} \Delta E_A^{HFS}(1S) &= 0.039(-13)(+3)(-0)(+22) \text{ meV}, \\ \Delta E_A^{HFS}(2S) &= 0.0049(-16)(+3)(+29)(-0) \text{ meV}. \end{aligned} \quad (13)$$

Comparing these results with those in Ref. [21], we find an opposite sign (and a factor of 2 difference) in the computation. As we can see from Table III, the doubly-virtual asymptotic behavior of the transition form factor plays an important role (about 50 %, between DIP and OPE models)^v and it has to be taken into account in any future estimation of ΔE_A^{HFS} .

Finally, incorporating the axial-vector mesons contributions in Eq. (13) along with the pseudoscalar one [38], $\Delta E_{HFS}^\pi = -(0.09 \pm 0.06) \mu\text{eV}$, we obtain

$$r_Z = 1.112(31)_{\text{exp}}(19)_{\text{th}}^{(+20)}(-10)_{\text{axials}}. \quad (14)$$

TABLE II. Results for the HFS of muonic hydrogen. The central values for the g_{ANN} couplings are those from ideal mixing ($\phi = 0$), Eq. (11). The second column displays results from OPE column in Table III, including as an additional uncertainty the difference with other models therein. The final two columns include uncertainties from $A_1(0)$, g_{ANN} , B_{2S} , m_A and an additional uncertainty from the mixing within brackets.

A	$\frac{A_1(0)}{\alpha^2 B_{2S}^A}$	$B_{2S}^A(0,0)$ [GeV $^{-2}$]	$\Delta E_A^{HFS}(1S)$ [meV]	$\Delta E_A^{HFS}(2S)$ [meV]
$f_1(1285)$	$1.53(25)(+00)(-20)$	0.269(30)	$0.011(2)(1)(1)(0)[0]$	$0.0014(-3)(+2)(1)(2)(0)[0]$
$a_1(1260)$	$1.41(30)(+00)(-27)$	0.245(63)	$0.029(+6)(-8)(6)(7)(2)[0]$	$0.0036(+8)(-10)(7)(9)(2)[0]$
$f_1(1420)$	$1.20(22)(+00)(-24)$	0.197(30)	$-0.001(0)(0)(0)(0)[+3]$	$-0.0001(0)(0)(0)(0)[+3]$
TOTAL			$0.039(-13)(+3)(-0)$	$0.0049(-16)(+3)(-0)$

TABLE III. The results for $A_1(0)/[\alpha^2 B_{2S}(0,0)]$ for $\ell = \mu$. For simplicity, we take ideal mixing in VMD models, implying that $m_V = 0.77$ GeV $\simeq m_{\rho,\omega}$ for a_1 , f_1 and $m_V = m_\phi$ for the f'_1 .

	VMD	eVMD	DIP	heVMD	heDIP	OPE
$f_1(1285)$	$1.68(27)$	$1.21(47)$	$0.99(17)$	$1.34(34)$	$1.33(48)$	$1.53(25)$
$a_1(1260)$	$1.68(27)$	$1.03(28)$	$0.91(20)$	$1.17(51)$	$1.14(53)$	$1.41(31)$
$f_1(1420)$	$2.99(35)$	$0.78(14)$	$0.78(15)$	$0.96(12)$	$0.96(33)$	$1.20(22)$

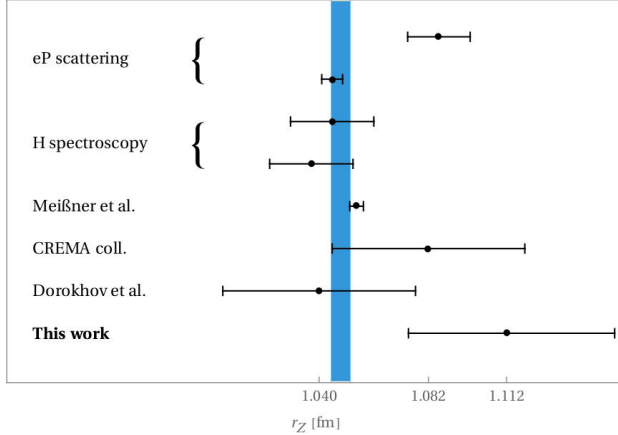


FIGURE 2. The Zemach radius (r_Z) from the references in the text and this work. The blue band represents the average from Refs. [39–42].

The value is in mild tension with other estimates, $r_Z = 1.086(12)$ fm [39] and $r_Z = 1.045(4)$ fm [40], from electron-proton scattering, $r_Z = 1.045(16)$ fm [41] and

$r_Z = 1.037(16)$ fm [42] from hydrogen spectroscopy, and $r_Z = 1.054(3)$ fm [43] from electron-proton scattering and e^+e^- annihilation. These outcomes are summarized in Fig. 2 where the blue band corresponds to the average for electron-proton (eP) scattering and hydrogen (H) spectroscopy.

Appendix

A. Form factors

In this contribution we assess the impact of the asymptotic behavior using different models for the $B_{2S}(q_1^2, q_2^2)$ form factor. For the doubly-virtual case, it is known that $B_{2S}(-Q^2, -Q^2) \sim \mathcal{O}(Q^{-4})$ for large Q^2 values [12, 15, 18, 44]. Besides, in the singly-virtual kinematic regime, it is also known from the light-cone expansion that, for large Q^2 values, $B_{2S}(-Q^2, -q^2) \sim \mathcal{O}(Q^{-4})$, where $q^2 \ll Q^2$ [18, 44], that is also suggested by L3 data [34, 35].

The models used in this work for the B_{2S} form factor are^{vi}:

$$B_{2S}^{\text{VMD}}(q_1^2, q_2^2) = \frac{B_{2S}(0, 0)m_V^4}{(q_1^2 - m_V^2)(q_2^2 - m_V^2)}, \quad (\text{A.1})$$

$$B_{2S}^{\text{eVMD/DIP}}(q_1^2, q_2^2) = \frac{B_{2S}(0, 0)m_V^4 M^4}{(q_1^2 - m_V^2)(q_1^2 - M^2)(q_2^2 - m_V^2)(q_2^2 - M^2)}, \quad (\text{A.2})$$

$$B_{2S}^{\text{OPE}}(q_1^2, q_2^2) = \frac{B_{2S}(0, 0)\Lambda_A^4}{(q_1^2 + q_2^2 - \Lambda_A^2)^2}, \quad (\text{A.3})$$

$$B_{2S}^{\text{he(VMD/DIP)}}(q_1^2, q_2^2) = B_{2S}^{\text{eVMD/DIP}}(q_1^2, q_2^2) [1 + q_1^2 q_2^2 \Lambda_{OPE}^{-4}]. \quad (\text{A.4})$$

For the normalization, we take the values for f_1, f'_1 from L3 [34, 35] together with the estimation in [12, 15] for the a_1 : $B_{2S}(0, 0) = \{0.269(30), 0.197(30), 0.245(63)\}\text{GeV}^{-2}$ for $\{f_1, f'_1, a_1\}$. Regarding the mass parameter, we take both, for the OPE and (he)DIP variants, $m_V = M = \Lambda_A = \{1.04(8), 0.926(79), 1.0(1)\}$ GeV, see Refs. [12, 15, 34, 35]. Concerning the eVMD and heVD models, we fix the M parameter to reproduce the slope from the L3 collaboration dipole in order to share the same low-energy behavior, which is accomplished adopting $M^2 = \Lambda_A^2 m_V^2 / (2m_V^2 - \Lambda_A^2) \sim 2$ GeV for $m_V = 0.77$ GeV. Finally, to ensure the OPE behavior in he(VMD/DIP) models, we find for ideal/L3 mixing $\Lambda_{OPE}^{f_1, f'_1, a_1} / m_V M = \{1.28(4)/1.37(5), 1.58(7)/1.26(6), 1.44(10)\}\text{GeV}^{-1}$, respectively.

Acknowledgements

A. M. wishes to thank the organizers for the pleasant conference. This work has been supported by the Spanish Ministry of Science and Innovation (grants SEV-2016-0588, FPA2017-86989-P and PID2020-112965GB-I00/AEI/10.13039/501100011033), by Secretaria d'Universitats i Recerca del Departament d'Economia i Coneixement de la Generalitat de Catalunya under (grant 2017SGR1069), and European Union's Horizon 2020 grants Research and Innovation Programme (grant no. 754510 (EU, H2020-MSCA-COFUND2016) and grant no. 824093 (H2020-INFRAIA-2018-1)). A. M. acknowledges Conacyt for his Ph. D. scholarship and P. R. the support of Cátedras Marcos Moshinsky (Fundación Marcos Moshinsky).

- i. Relations to other bases can be found in [12, 25].
 - ii. Here, L stands for longitudinal.
 - iii. At this order, B_{2S} becomes the only relevant form factor.
 - iv. We further note that, for the dipole (DIP) parametrization employed in Ref. [21], $A_1(0) = (4/3)(\alpha/\pi)^2 B_{2S}(0,0)I(m_\ell)$, with $I(m_\ell)$ defined in the Eq. (27) from Ref. [21].
 - v. From Table III, we can see an effect of about 10% (20%) for the eVMD (DIP) model compared with the heVMD (heDIP) one, which has been corrected to comply with the asymptotic behavior of the transition form factors, making explicit the relevance of the low-energy behavior of the TFFs.
 - vi. Further details can be found in [25].
1. G. W. Bennett *et al.* [Muon g-2], “Final Report of the Muon E821 Anomalous Magnetic Moment Measurement at BNL,” *Phys. Rev. D* **73** (2006) 072003, <https://doi.org/10.1103/PhysRevD.73.072003>.
 2. B. Abi *et al.* [Muon g-2], “Measurement of the Positive Muon Anomalous Magnetic Moment to 0.46 ppm,” *Phys. Rev. Lett.* **126** (2021) 141801, <https://doi.org/10.1103/PhysRevLett.126.141801>.
 3. R. Aaij *et al.* [LHCb], “Test of lepton universality in beauty-quark decays,” *Nature Phys.* **18** (2022) 277, <https://doi.org/10.1038/s41567-021-01478-8>.
 4. B. Capdevila, A. Crivellin, S. Descotes-Genon, J. Matias and J. Virto, “Patterns of New Physics in $b \rightarrow s\ell^+\ell^-$ transitions in the light of recent data,” *JHEP* **01** (2018) 093, [https://doi.org/10.1007/JHEP01\(2018\)093](https://doi.org/10.1007/JHEP01(2018)093).
 5. J. Aebischer, W. Altmannshofer, D. Guadagnoli, M. Reboud, P. Stangl and D. M. Straub, “ B -decay discrepancies after Moriond 2019,” *Eur. Phys. J. C* **80** (2020) 252, <https://doi.org/10.1140/epjc/s10052-020-7817-x>.
 6. A. Antognini *et al.*, “Proton Structure from the Measurement of $2S - 2P$ Transition Frequencies of Muonic Hydrogen,” *Science* **339** (2013) 417, <https://doi.org/10.1126/science.1230016>.
 7. Y. Ma *et al.*, “New Precision Measurement for Proton Zemach Radius with Laser Spectroscopy,” *Int. J. Mod. Phys. Conf. Ser.* **40** (2016) 1660046, <https://doi.org/10.1142/S2010194516600466>.
 8. R. Pohl [CREMA], “Laser Spectroscopy of Muonic Hydrogen and the Puzzling Proton,” *J. Phys. Soc. Jap.* **85** (2016) 091003, <https://doi.org/10.7566/JPSJ.85.091003>.
 9. A. Adamczak *et al.* [FAMU], “Steps towards the hyperfine splitting measurement of the muonic hydrogen ground state: pulsed muon beam and detection system characterization,” *JINST* **11** (2016) P05007, <https://doi.org/10.1088/1748-0221/11/05/P05007>.
 10. V. Pauk and M. Vanderhaeghen, “Single meson contributions to the muon’s anomalous magnetic moment,” *Eur. Phys. J. C* **74** (2014) 3008, <https://doi.org/10.1140/epjc/s10052-014-3008-y>.
 11. F. Jegerlehner, “The Anomalous Magnetic Moment of the Muon,” *Springer Tracts Mod. Phys.* **274** (2017) 1, <https://doi.org/10.1007/978-3-319-63577-4>.
 12. P. Roig and P. Sanchez-Puertas, “Axial-vector exchange contribution to the hadronic light-by-light piece of the muon anomalous magnetic moment,” *Phys. Rev. D* **101** (2020) 074019, <https://doi.org/10.1103/PhysRevD.101.074019>.
 13. J. Leutgeb and A. Rebhan, “Axial vector transition form factors in holographic QCD and their contribution to the anomalous magnetic moment of the muon,” *Phys. Rev. D* **101** (2020) 114015, <https://doi.org/10.1103/PhysRevD.101.114015>.
 14. L. Cappiello, O. Catà, G. D’Ambrosio, D. Greynat and A. Iyer, “Axial-vector and pseudoscalar mesons in the hadronic light-by-light contribution to the muon ($g - 2$),” *Phys. Rev. D* **102** (2020) 016009, <https://doi.org/10.1103/PhysRevD.102.016009>.
 15. P. Masjuan, P. Roig and P. Sanchez-Puertas, “The interplay of transverse degrees of freedom and axial-vector mesons with short-distance constraints in $g - 2$,” *J. Phys. G* **49** (2022) 015002, <https://doi.org/10.1088/1361-6471/ac3892>.
 16. T. Aoyama, N. Asmussen, M. Benayoun, J. Bijnens, T. Blum, M. Bruno, I. Caprini, C. M. Carloni Calame, M. Cè and G. Colangelo, *et al.*, “The anomalous magnetic moment of the muon in the Standard Model,” *Phys. Rept.* **887** (2020) 1, <https://doi.org/10.1016/j.physrep.2020.07.006>.
 17. A. Szczurek, “Production of axial-vector mesons at e^+e^- collisions with double-tagging as a way to constrain the axial meson light-by-light contribution to the muon g-2 and the hyperfine splitting of muonic hydrogen,” *Phys. Rev. D* **102** (2020) 113015, <https://doi.org/10.1103/PhysRevD.102.113015>.
 18. M. Zanke, M. Hoferichter and B. Kubis, “On the transition form factors of the axial-vector resonance $f_1(1285)$ and its decay into e^+e^- ,” *JHEP* **07** (2021) 106, [https://doi.org/10.1007/JHEP07\(2021\)106](https://doi.org/10.1007/JHEP07(2021)106).
 19. G. Colangelo, F. Hagelstein, M. Hoferichter, L. Laub and P. Stoffer, “Short-distance constraints for the longitudinal component of the hadronic light-by-light amplitude: an update,” *Eur. Phys. J. C* **81** (2021) 702, <https://doi.org/10.1140/epjc/s10052-021-09513-x>.
 20. J. Leutgeb and A. Rebhan, “Hadronic light-by-light contribution to the muon g-2 from holographic QCD with massive pions,” *Phys. Rev. D* **104** (2021) 094017, <https://doi.org/10.1103/PhysRevD.104.094017>.
 21. A. E. Dorokhov, N. I. Kochelev, A. P. Martynenko, F. A. Martynenko and A. E. Radzhabov, “The contribution of axial-vector mesons to hyperfine structure of muonic hydrogen,” *Phys. Lett. B* **776** (2018) 105, <https://doi.org/10.1016/j.physletb.2017.11.027>.
 22. P. Masjuan, E. Ruiz Arriola and W. Broniowski, “Meson dominance of hadron form factors and large- N_c phenomenology,” *Phys. Rev. D* **87** (2013) 014005, <https://doi.org/10.1103/PhysRevD.87.014005>.
 23. A. E. Dorokhov, A. P. Martynenko, F. A. Martynenko and A. E. Radzhabov, “Effects of light-by-light scattering in the Lamb shift and hyperfine structure of muonic hydrogen,” *EPJ Web Conf.* **222** (2019) 03010, <https://doi.org/10.1051/epjconf/201922203010>.

24. A. S. Rudenko, “ $f_1(1285) \rightarrow e^+e^-$ decay and direct f_1 production in e^+e^- collisions,” *Phys. Rev. D* **96** (2017) 076004, <https://doi.org/10.1103/PhysRevD.96.076004>.
25. A. Miranda, P. Roig and P. Sanchez-Puertas, “Axial-vector exchange contribution to the hyperfine splitting,” *Phys. Rev. D* **105** (2022) 016017, <https://doi.org/10.1103/PhysRevD.105.016017>.
26. M. N. Achasov *et al.* [SND], “Search for direct production of the $f_1(1285)$ resonance in e^+e^- collisions,” *Phys. Lett. B* **800** (2020) 135074, <https://doi.org/10.1016/j.physletb.2019.135074>.
27. L. D. Landau, “On the angular momentum of a system of two photons,” *Dokl. Akad. Nauk SSSR* **60** (1948) 207, <https://doi.org/10.1016/B978-0-08-010586-4.50070-5>.
28. C. N. Yang, “Selection Rules for the Dematerialization of a Particle Into Two Photons,” *Phys. Rev.* **77** (1950) 242, <https://doi.org/10.1103/PhysRev.77.242>.
29. C. Frugueule and C. Peset, “Muonic vs electronic dark forces: a complete EFT treatment for atomic spectroscopy,” [[arXiv:2107.13512 \[hep-ph\]](https://arxiv.org/abs/2107.13512)].
30. L. Hayen, “Radiative corrections to nucleon weak charges and Beyond Standard Model impact,” [[arXiv:2102.03458 \[hep-ph\]](https://arxiv.org/abs/2102.03458)].
31. C. Alexandrou *et al.*, “Nucleon axial, tensor, and scalar charges and σ -terms in lattice QCD,” *Phys. Rev. D* **102** (2020) 054517, <https://doi.org/10.1103/PhysRevD.102.054517>.
32. D. G. Dumm, P. Roig, A. Pich and J. Portoles, “ $\tau \rightarrow \pi \pi \nu(\tau)$ decays and the $a(1)(1260)$ off-shell width revisited,” *Phys. Lett. B* **685** (2010) 158, <https://doi.org/10.1016/j.physletb.2010.01.059>.
33. I. M. Nugent, T. Przedzinski, P. Roig, O. Shekhovtsova and Z. Was, “Resonance chiral Lagrangian currents and experimental data for $\tau^- \rightarrow \pi^-\pi^-\pi^+\nu_\tau$,” *Phys. Rev. D* **88** (2013) 093012, <https://doi.org/10.1103/PhysRevD.88.093012>.
34. P. Achard *et al.* [L3], “ $f_1(1285)$ formation in two photon collisions at LEP,” *Phys. Lett. B* **526** (2002) 269, [https://doi.org/10.1016/S0370-2693\(01\)01477-0](https://doi.org/10.1016/S0370-2693(01)01477-0).
35. P. Achard *et al.* [L3], “Study of resonance formation in the mass region 1400-MeV to 1500-MeV through the reaction gamma gamma $\rightarrow K0(S) K^+ \pi^-$,” *JHEP* **03** (2007) 018, <https://doi.org/10.1088/1126-6708/2007/03/018>.
36. P. A. Zyla *et al.* [Particle Data Group], “Review of Particle Physics,” *PTEP* **2020** (2020) 083C01, <https://doi.org/10.1093/ptep/ptaa104>.
37. P. Masjuan, E. Ruiz Arriola and W. Broniowski, “Systematics of radial and angular-momentum Regge trajectories of light non-strange q-barq-states,” *Phys. Rev. D* **85** (2012) 094006, <https://doi.org/10.1103/PhysRevD.85.094006>.
38. N. T. Huong, E. Kou and B. Moussallam, “Single pion contribution to the hyperfine splitting in muonic hydrogen,” *Phys. Rev. D* **93** (2016) 114005, <https://doi.org/10.1103/PhysRevD.93.114005>.
39. J. L. Friar and I. Sick, “Zemach moments for hydrogen and deuterium,” *Phys. Lett. B* **579** (2004) 285, <https://doi.org/10.1016/j.physletb.2003.11.018>.
40. M. O. Distler, J. C. Bernauer and T. Walcher, “The RMS Charge Radius of the Proton and Zemach Moments,” *Phys. Lett. B* **696** (2011) 343-347. <https://doi.org/10.1016/j.physletb.2010.12.067>.
41. A. V. Volotka, V. M. Shabaev, G. Plunien and G. Soff, “Zemach and magnetic radius of the proton from the hyperfine splitting in hydrogen,” *Eur. Phys. J. D* **33** (2005) 23-27. <https://doi.org/10.1140/epjd/e2005-00025-9>.
42. A. Dupays, A. Beswick, B. Lepetit, C. Rizzo and D. Bakalov, “Proton Zemach radius from measurements of the hyperfine splitting of hydrogen and muonic hydrogen,” *Phys. Rev. A* **68** (2003) 052503. <https://doi.org/10.1103/PhysRevA.68.052503>.
43. Y. H. Lin, H. W. Hammer and U. G. Meißner, “New Insights into the Nucleon’s Electromagnetic Structure,” *Phys. Rev. Lett.* **128** (2022) 052002, <https://doi.org/10.1103/PhysRevLett.128.052002>. [[arXiv:2109.12961 \[hep-ph\]](https://arxiv.org/abs/2109.12961)].
44. M. Hoferichter and P. Stoffer, “Asymptotic behavior of meson transition form factors,” *JHEP* **05** (2020) 159, [https://doi.org/10.1007/JHEP05\(2020\)159](https://doi.org/10.1007/JHEP05(2020)159). [[arXiv:2004.06127 \[hep-ph\]](https://arxiv.org/abs/2004.06127)].